Forschungszentrum Jülich

Programmgruppe Systemforschung
und Technologische Entwicklung

Change Detection with High-Resolution Satellite Imagery in Support of Verification and Crisis Prevention: Nuclear Applications

Morton John Canty

Jül-3842

Change Detection with High-Resolution Satellite Imagery in Support of Verification and Crisis Prevention: Nuclear Applications

Morton John Canty

Berichte des Forschungszentrums Jülich ; 3842
ISSN 0944-2952
Programmgruppe Systemforschung und Technologische Entwicklung Jül-3842

Zu beziehen durch: Forschungszentrum Jülich GmbH · Zentralbibliothek
52425 Jülich · Bundesrepublik Deutschland
☎ 02461/61-5220 · Telefax: 02461/61-6103 · e-mail: zb-publikation@fz-juelich.de

Change Detection with High-Resolution Satellite Imagery in Support of Verification and Crisis Prevention: Nuclear Applications*

M. J. Canty
Forschungszentrum Jülich GmbH
D-52425 Jülich, Germany

*Gefördert durch das Bundesministerium für Bildung und Forschung im Rahmen der Friedens- und Konfliktforschung, Förderkennzeichen: 01 LX 9909/1

Abstract: The applicability to nuclear verification of statistical change detection methods for commercial, multispectral satellite imagery is investigated. Case studies relating to international treaties on nuclear disarmament and non-proliferation are described.

Contents

1 Introduction

A potential application of the presently available, medium and high-resolution imagery from commercial earth observation satellites to verification of peaceful and military nuclear activities involves *wide area change detection.* The idea is to try to pinpoint automatically those parts of a fairly large scene in which significant changes have taken place, which can then be screened with other information for further, more detailed investigation. Much of the multitemporal satellite data available is also multispectral in nature (LANDSAT, SPOT, IRS, IKONOS) so that methods that make optimal use of all spectral channels simultaneously are of particular interest.

In this report, we describe the application of an advanced statistical change detection technique to nuclear verification, called *multivariate alteration detection* (MAD), proposed recently by Alan Nielsen and co-workers [1] and implemented as part of a satellite image analysis system developed at the Jülich Research Center. These investigations have been carried out in the framework of a peace research project funded by the German Federal Ministry for Education and Research.

We begin in Section 2 with a technical description of the change detection algorithm. Then, in Section 3, several case studies are described which the span three relevant nuclear verification regimes, namely the Comprehensive Test Ban Treaty (CTBT), the Nuclear Non-Proliferation Treaty (NTP) and a future Fissile Materials Cutoff Treaty (FMCT). Conclusions are presented in Section 4. A brief description of the software product and a list publications emanating from the project are given in appendices.

2 Multivariate alteration detection

A multispectral image taken at some time t_1 has N components or bands. We can represent the gray value of a "typical" pixel in one of these components with the symbol X_i, where $i = 1 \dots N$. Technically X_i is a *random variable* and $X = (X_1, X_2 \dots X_N)$ is a *random vector* corresponding to the measurement at the satellite sensors of the reflected solar radiation. The pixel intensities for an image of the same scene taken at a later time t_2 can similarly be represented by $Y = (Y_1, Y_2 \dots Y_N)$.

2.1 Theory

In order to see changes in the two images, a simple procedure would be to subtract them from each other component-by-component. One could then examine the N differenced images characterized by

$$X - Y = (X_1 - Y_1, X_2 - Y_2 \dots X_N - Y_N)$$

for significant changes. Pixel intensities near zero indicate no change, large positive or negative values indicate change, and decision thresholds can be set to define significant changes. There is a better way to proceed, however. Suppose we make a *linear combination* of the intensities for all N channels in the first image, that is we create a *single* image whose pixel intensities are

$$U = a_1X_1 + a_2X_2 + \dots a_NX_N,$$

where the coefficients a_i are as yet unspecified. We do the same for t_2, i.e.

$$V = b_1Y_1 + b_2Y_2 + \dots b_NY_N,$$

and then look at the single differenced image $U - V$.

The advantage of this procedure is that it combines all the information into a single image, and one is free to choose the coefficients a_i and b_i in any suitable way. The MAD procedure determines the coefficients so that the *positive correlation between U and V is minimized.* This means that the resulting differenced image $U - V$ will show maximum spread in its pixel intensities. If we assume that the spread is primarily due to actual changes that have taken place in the scene over the interval t_2-t_1, then this procedure will enhance those changes as much as possible.

In more convenient vector notation, we seek linear combinations

$$U = a^\top X, \quad V = b^\top Y$$

such that the difference of the transformed vectors has maximum variance:

$$\mathrm{var}(U - V) = \mathrm{var}(U) + \mathrm{var}(V) - 2\mathrm{cov}(U, V) \to \text{maximum},$$

subject to the constraints

$$\mathrm{var}(U) = \mathrm{var}(V) = 1. \tag{1}$$

Note that under these constraints

$$\mathrm{var}(U - V) = 2(1 - \mathrm{corr}(U, V)). \tag{2}$$

Since we are dealing with change detection, we require that the random variables u and v be positively correlated, that is

$$\mathrm{cov}(U, V) = \mathrm{cov}(a^\top X, b^\top Y) > 0.$$

We seek vectors a and b which *minimize* the positive covariance $\mathrm{cov}(U, V)$ under the constraints (1).

Without loss of generality we can assume that the expected values of X and Y are nil. Then for multivariate normally distributed data the combined random vector is distributed as

$$\begin{pmatrix} X \\ Y \end{pmatrix} \sim N\left[\begin{pmatrix} 0 \\ 0 \end{pmatrix}, \begin{pmatrix} \Sigma_{xx} & \Sigma_{xy} \\ \Sigma_{yx} & \Sigma_{yy} \end{pmatrix}\right]. \tag{3}$$

With the definition of variance we have

$$\mathrm{var}(U) = a^\top \Sigma_{xx} a, \quad \mathrm{var}(V) = b^\top \Sigma_{yy} b.$$

Introducing the Lagrange multipliers $\nu/2$ and $\mu/2$, maximizing the covariance $\mathrm{cov}(U, V)$ under the constraints (1) is equivalent to maximizing the unconstrained Lagrange function

$$L = a^\top \Sigma_{xy} b - \frac{\nu}{2}(a^\top \Sigma_{xx} a - 1) - \frac{\mu}{2}(b^\top \Sigma_{yy} b - 1).$$

Differentiating, we obtain

$$\frac{\partial L}{\partial a} = \Sigma_{xy} b - \frac{\nu}{2} 2\Sigma_{xx} a = 0$$
$$\frac{\partial L}{\partial b} = \Sigma_{xy} a - \frac{\mu}{2} 2\Sigma_{yy} b = 0$$

or

$$a = \frac{1}{\nu}\Sigma_{xx}^{-1}\Sigma_{xy} b, \quad b = \frac{1}{\mu}\Sigma_{yy}^{-1}\Sigma_{xy} a.$$

The correlation between the random vectors U and V is

$$\rho = \frac{\mathrm{cov}(U, V)}{\sqrt{\mathrm{var}(U)\mathrm{var}(V)}} = \frac{a^\top \Sigma_{xy} b}{\sqrt{a^\top \Sigma_{xx} a \; b^\top \Sigma_{yy} b}}. \tag{4}$$

Substituting for a and b in this equation gives (with $\Sigma_{xy}^\top = \Sigma_{yx}$)

$$\rho^2 = \frac{a^\top \Sigma_{xy} \Sigma_{yy}^{-1} \Sigma_{yx} a}{a^\top \Sigma_{xx} a}$$
$$\rho^2 = \frac{b^\top \Sigma_{yx} \Sigma_{xx}^{-1} \Sigma_{xy} b}{b^\top \Sigma_{yy} b},$$

which are equivalent to the two *generalized eigenvalue problems*

$$\begin{aligned}\Sigma_{xy}\Sigma_{yy}^{-1}\Sigma_{yx}a &= \rho^2\Sigma_{xx}a\\ \Sigma_{yx}\Sigma_{xx}^{-1}\Sigma_{xy}b &= \rho^2\Sigma_{yy}b.\end{aligned} \tag{5}$$

Thus the desired projections $u = a^\top X$ are given by the eigenvectors $a^1 \ldots a^N$ corresponding to the generalized eigenvalues

$$\rho^2 \sim \lambda^1 \geq \ldots \geq \lambda^N$$

of $\Sigma_{xy}\Sigma yy^{-1}\Sigma_{yx}$ with respect to Σ_{xx}. Similarly the desired projections $v = b^\top Y$ are given by the eigenvectors $b^1 \ldots b^N$ of $\Sigma_{yx}\Sigma xx^{-1}\Sigma_{xy}$ with respect to Σ_{yy} corresponding to the *same* eigenvalues. Under these transformations, we can write (2) as

$$\mathrm{var}(U - V) = 2(1-\rho) \;\sim\; 2(1-\sqrt{\lambda^p}), \quad p = 1 \ldots N.$$

The transformation corresponding to the smallest eigenvalue, namely (a^N, b^N) will thus give maximal variance for the difference $U - V$. Nielsen et al. [1] refer to the N difference components

$$U^p - V^p \;=\; a^{p\top}X - b^{p\top}Y, \quad p = 1 \ldots N, \tag{6}$$

as the *multivariate alteration detection* (MAD) components of the combined bitemporal image.

The MAD transformation calculations run completely automatically and are determined solely by the statistical properties (spectral dispersion matrices) of the image data. There are no adjustable parameters involved. They return the difference images $MAD^p = U^p - V^p$ along with their standard deviations σ^p_{MAD}, $p = 1 \ldots N$. Fig. 1 shows a typical scatter plot of MAD^1 vs. MAD^2 for two LANDSAT images. The components are seen to be uncorrelated and approximately Gaussian.

The last MAD component MAD^N has maximum spread in its pixel intensities and, ideally, maximum change information. However, depending on the type of change one is looking for, the other differenced images may also be extremely useful. The second-to-last image has maximum spread subject to the condition that the pixel intensities are *statistically uncorrelated* with those in the first image, and so on. Since interesting anthropomorphic changes will generally be uncorrelated with dominating seasonal vegetation changes or stochastic image noise, it is quite common that such changes will be concentrated in higher order components. This in fact is one of the nicest

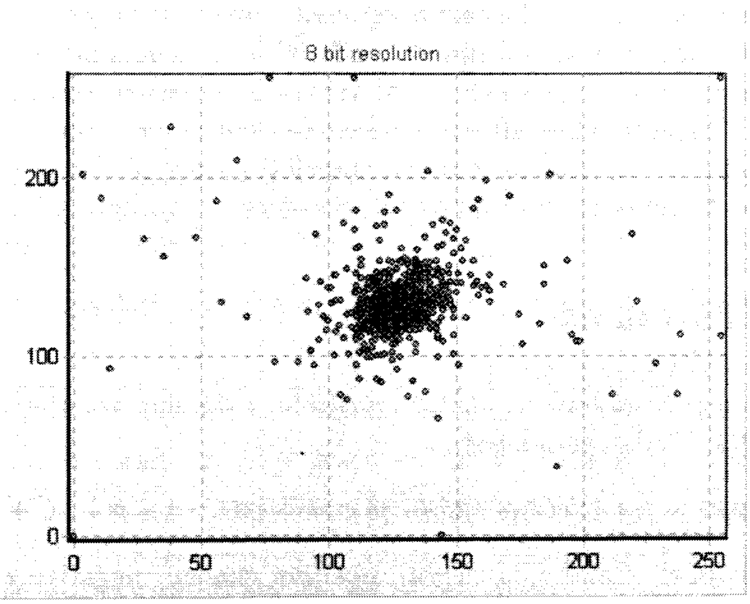

Figure 1: Typical scatter plot of the first two MAD components for bitemporal LANDSAT imagery.

aspects of the method: It sorts different categories of change into different image components.

For an alternative statistical change detection algorithm, based on iterative principle components analysis, see Wiemker et al. [2].

2.2 Invariance properties

An additional advantage of the MAD procedure stems from the fact that the calculations involved are invariant under linear transformations of the original image intensities. This implies that the method is insensitive to differences in atmospheric conditions or sensor calibrations at the two acquisition times. If for example the pixel intensities Y in the later image are transformed linearly according to

$$Y \rightarrow AY,$$

where A is any $N \times N$ real matrix, then we can write

$$V = b^\top AY = c^\top Y.$$

where $c = A^\top b$. Then the same arguments follow through, and equations (5) remain unchanged with b simply replaced by c. The generalized eigenvalues and eigenvectors, and hence the MAD transformation itself, are the same as before. Changes in overall atmospheric absorption or in sensor calibration are approximately equivalent to linear transformations of the pixel intensities, so that the MAD procedure tends to be insensitive to both of these effects.

2.3 Thresholds

We consider the following *mixture model* for a random variable X representing one of the MAD components:

$$p(x) = p(x \mid NC)p(NC) + p(x \mid C-)p(C-) + p(x \mid C+)p(C+), \qquad (7)$$

where $C+$, $C-$ and NC denote positive change, negative change and no change, respectively. The set of measurements $S = \{x_i\}$ may be grouped into four disjoint sets:

$$S_{NC}, \quad S_{C-}, \quad S_{C+}, \quad S_U = S \backslash S_{NC} \cup S_{C-} \cup S_{C+},$$

with S_U denoting the set of ambiguous pixels.[1] From the sample mean and sample variance, we estimate initially the moments for the distribution of no-change pixels:

$$\mu_{NC} = \frac{1}{|S_{NC}|} \cdot \sum_{i \in S_{NC}} x_i,$$

$$(\sigma_{NC})^2 = \frac{1}{|S_{NC}|} \cdot \sum_{i \in S_{NC}} (x_i - \mu_{NC})^2$$

($|S|$ denotes set cardinality) and similarly for $C-$ and $C+$. Bruzzone and Prieto [3] suggest improving these estimates by using the pixels in S_U and applying the so-called *EM algorithm* (see [4] for a good explanation):

$$\begin{aligned} \mu'_{NC} &= \sum_{i \in S} p(NC \mid x_i) x_i \;/\; \sum_{i \in S} p(NC \mid x_i) \\ (\sigma'_{NC})^2 &= \sum_{i \in S} p(NC \mid x_i)(x_i - \mu'_{NC})^2 \;/\; \sum_{i \in S} p(NC \mid x_i) \\ p'(NC) &= \frac{1}{|S|} \cdot \sum_{i \in S} p(NC \mid x_i) \,, \end{aligned} \qquad (8)$$

[1] The symbols $\cup$ and $\backslash$ denote set union and set difference, respectively. These sets can be determined in practice by setting generous, scene-independent thresholds for change and no-change pixel intensities, see [3].

where $P(NC \mid x_i)$ is the *a posteriori* probability for a no-change pixel conditional on measurement x_i. We have the following rules for determining $P(NC \mid x_i)$:

1. $i \in S_{NC}$: $\quad p(NC \mid x_i) = 1$
2. $i \in S_{C\pm}$: $\quad p(NC \mid x_i) = 0$
3. $i \in S_U$: $\quad p(NC \mid x_i) = p(x_i \mid NC)p(NC)/p(x_i)$ (Bayes' rule),

$$\text{where} \quad p(x_i \mid NC) = \frac{1}{2\pi\sigma_{NC}^2} \cdot \exp\left(\frac{-(x_i - \mu_{NC})^2}{2\sigma_{NC}^2}\right)$$

$$\text{and} \quad p(x_i) = p(x_i \mid NC)p(NC) + p(x_i \mid C-)p(C-) + p(x_i \mid C+)p(C+).$$

Substituting into (8) we obtain the set of equations

$$\mu'_{NC} = \frac{\sum_{i \in S_U} p(NC \mid x_i)x_i + \sum_{i \in S_{NC}} x_i}{\sum_{i \in S_U} p(NC \mid x_i) + |S_{NC}|}$$

$$(\sigma'_{NC})^2 = \frac{\sum_{i \in S_U} p(NC \mid x_i)(x_i - \mu'_{NC})^2 + \sum_{i \in S_{NC}} (x_i - \mu'_{NC})^2}{\sum_{i \in S_U} p(NC \mid x_i) + |S_{NC}|}$$

$$p'(NC) = \frac{1}{|S|}\left(\sum_{i \in S_U} p(NC \mid x_i) + |S_{NC}|\right),$$

which can be iterated numerically to improve the initial estimates of the distributions. One can then determine e.g. the upper change threshold as the appropriate solution of

$$p(x \mid NC)p(NC) = p(x \mid C+)p(C+).$$

Taking logarithms,

$$\frac{1}{2\sigma_{C+}^2}(x - \mu_{C+})^2 - \frac{1}{2\sigma_{NC}^2}(x - \mu_{NC})^2 = \log\left[\frac{\sigma_{NC}^2}{\sigma_{C+}^2} \cdot \frac{p(C+)}{P(NC)}\right] =: A$$

with solutions

$$x = \frac{\mu_{C+}\sigma_{NC}^2 - \mu_{NC}\sigma_{C+}^2 \pm \sigma_{NC}\sigma_{C+}\sqrt{(\mu_{NC} - \mu_{C+})^2 + 2A(\sigma_{NC}^2 - \sigma_{C+}^2)}}{\sigma_{NC}^2 - \sigma_{C+}^2}.$$

A corresponding expression obtains for the lower threshold.

2.4 Registration

The most tedious task associated with change detection is the registration of the images involved, in particular the setting of ground control points (GCPs). It is essential that registration be carried through at sub-pixel accuracy, to avoid as much as possible false change signals. In general, it is necessary to resort to the manual entry of GCPs. However various techniques for their automatic determination have been suggested in the literature. We have implemented two such methods, namely contour matching [5] and corner detection [6] in our change detection software. These techniques have been found to function very reliably in bitemporal scenes in which vegetation changes do not dominate (e.g. nuclear test sites, which are often located in remote, arid regions). They can of course be augmented (or replaced) by manual determination. All image registrations involved in this report, whether with automatically or manually determined GCPs, are carried out with first, second or third order polynomial nearest-neighbor resampling (see Richards [7]).

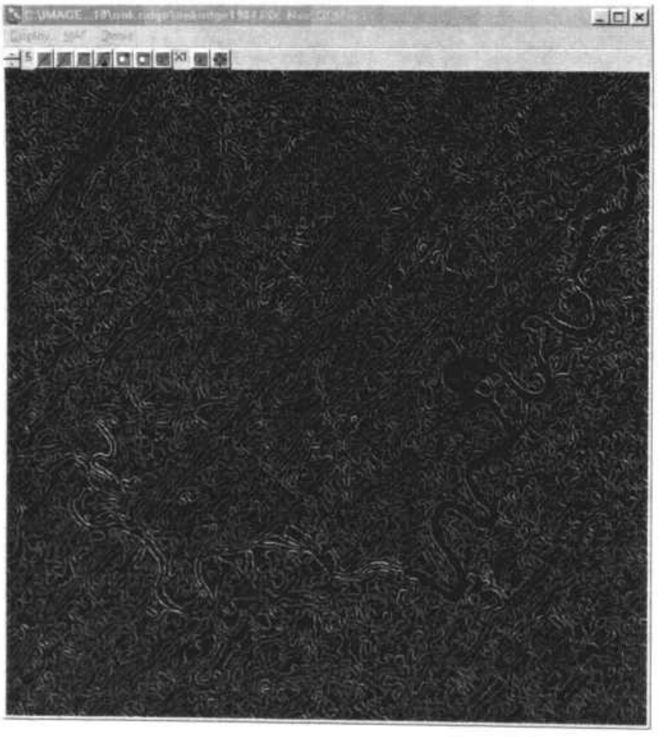

Figure 2: Raw contours from the Log-of-Gaussian filter.

Contour matching is illustrated in Figures 2 – 4. Fig. 2 shows the raw contours obtained from a so-called *Log-of-Guassian* filter applied to a master image. Fig. 3 shows the significant closed contours derived therefrom, and Fig. 4 displays the GCPs determined from the match between master and slave images.

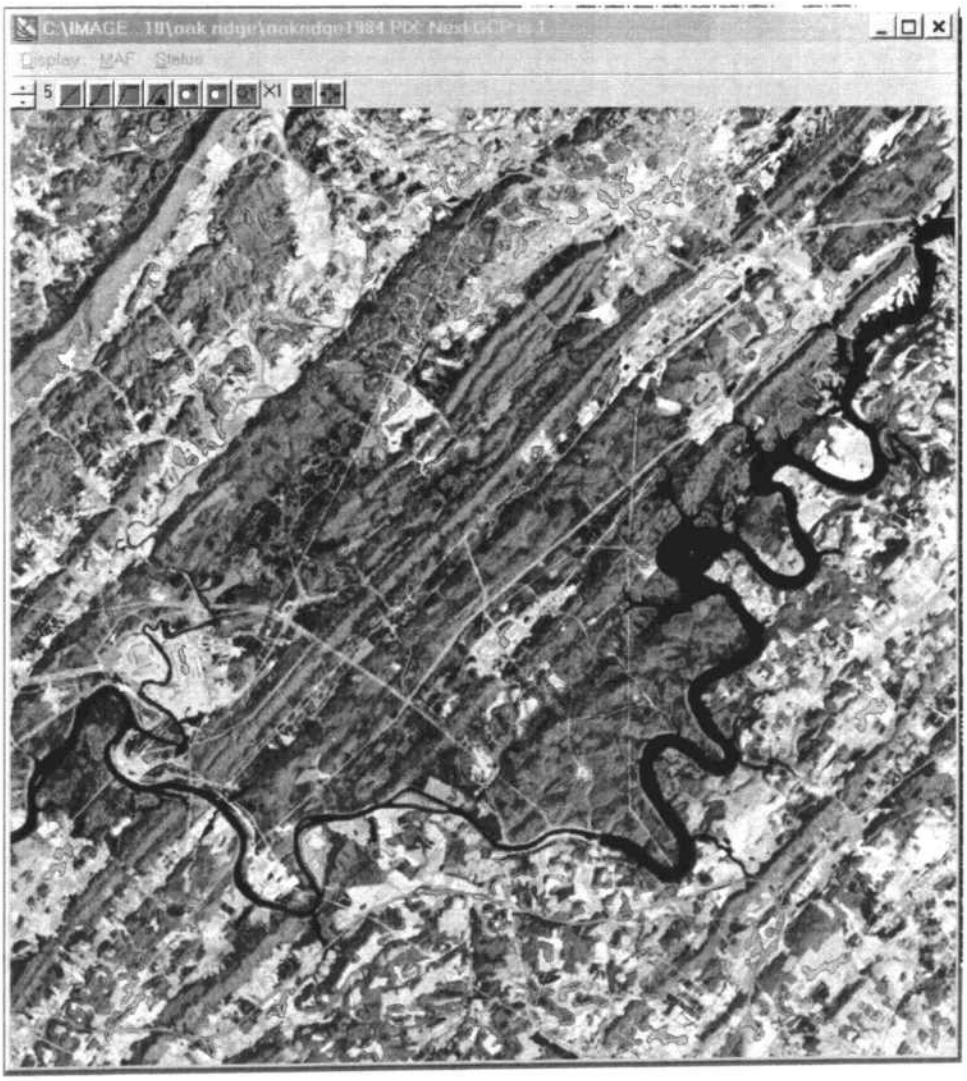

Figure 3: Significant closed contours from Fig. 2.

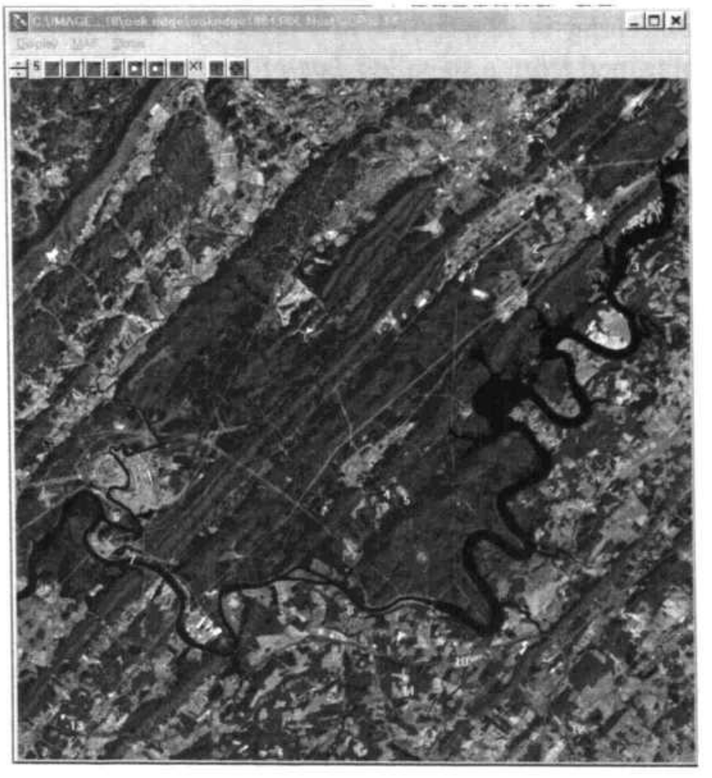

Figure 4: Matched ground control points.

3 Case studies

3.1 CTBT verification

The use of remote sensing satellite imagery is not foreseen as a routine verification measure for the Comprehensive Test Ban Treaty (CTBT). Nevertheless member States to the treaty may support the verification activities of the central control authority (CTBO) with their so-called *national technical means* (NTM). These may include the analysis of satellite data. We illustrate the potential use of such data, in particular the application of change detection, with two case studies.

3.1.1 Pokaran

The following investigation was carried out in collaboration with Joerg Schlittenhardt, Federal Institute for Geosciences and Natural Resources, Hannover and under consultation with Bhupendra Jasani, Dept. of War Studies, King's College, London.

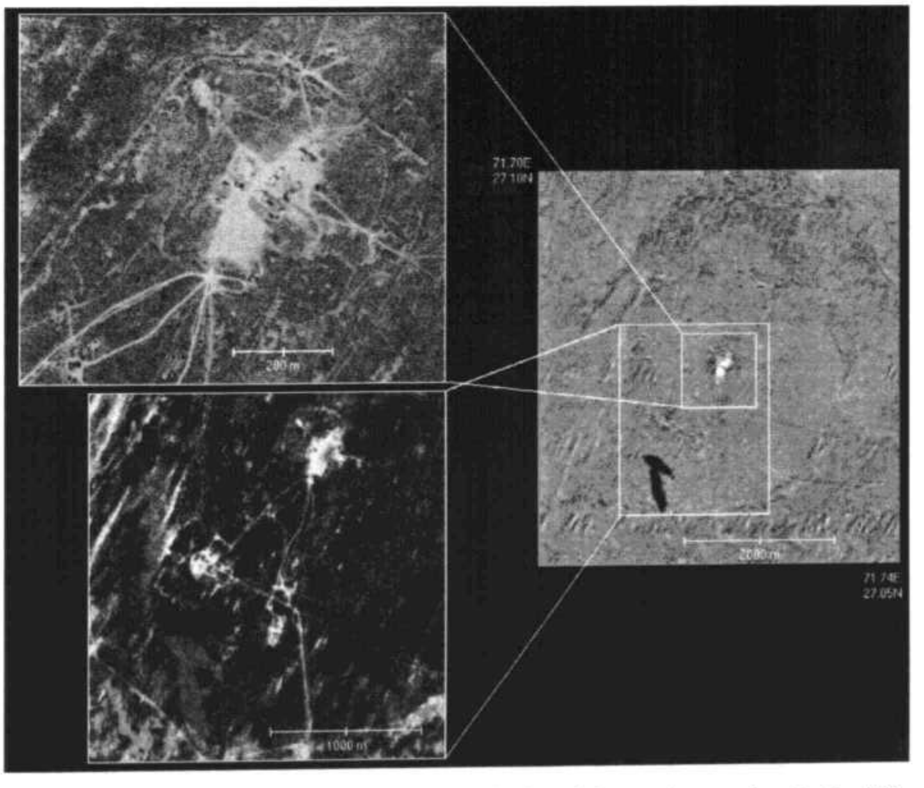

Figure 5: Change detection results. The right hand inset shows the sixth difference component for two multispectral Landsat images acquired over the Pokaran test area on March 29 and May 16, 1998. Pixel intensities differing from middle gray (Digital Number=127 on a scale of 0 to 255) indicate degree of change. The upper left insert is taken from a KVR-1000 image acquired on Feb. 2, 1998. The lower left insert shows a contrast enhanced and magnified portion of a SPOT panchromatic image acquired on May 13, 1998.

In May 1998 India and Pakistan each conducted two series of underground nuclear explosions. Shortly after the tests had been conducted, detailed information about the test programme, including number and type of explosions and their TNT equivalent, were released by the Indian and Pakistani governments and their respective agencies. In particular, India claimed to have carried out 3 simultaneous tests on May 11 with a combined yield of 55 kt TNT, and two further tests on May 13 with a yield of 0.8 kt TNT. The fact that not all of the announced explosions were detected by the International Monitoring System (IMS) and the discrepancies that arose between the subsequently calculated seismic yield and the "announced" yield triggered several critical articles in a number of scientific journals. Questions were raised as to the reliability of seismic verification and particularly of the IMS, which is being set up to monitor compliance with the CTBT.

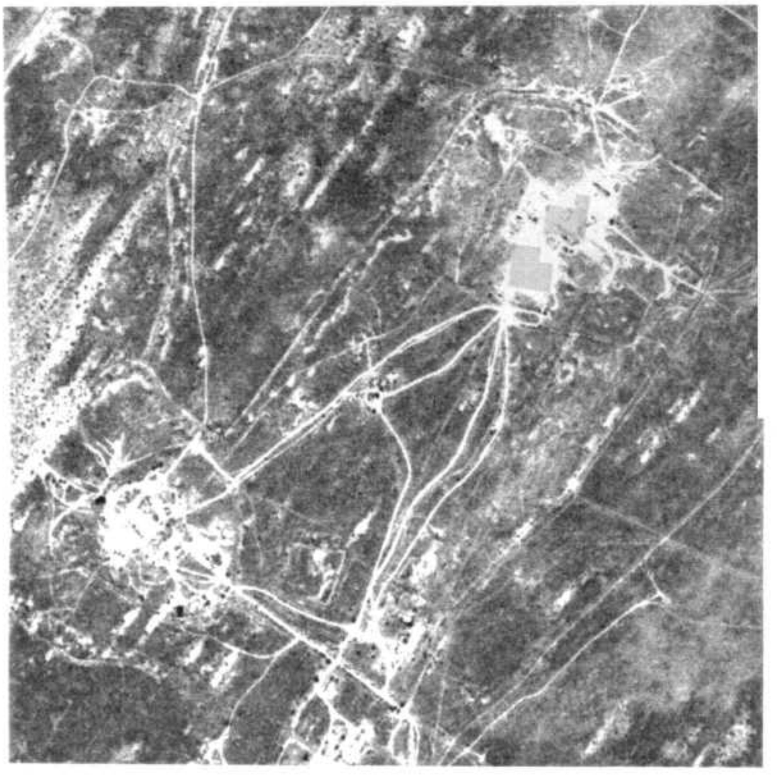

Figure 6: Cutout from the KVR-1000 image acquired on Feb. 2, 1998 with change detection.

The result of an application of the change detection method to two LANDSAT images over the Pokaran test area in the Rajasthan Desert, acquired approximately 6 weeks before and a few days after the alleged underground tests of May, 1998, is shown in Fig. 5. The right hand insert shows the first difference component MAD^1, in which the changes were most evident. Three significant changes can be seen, two of which are very close together and located at what appears to be a plausible test site, see also Fig. 6. These latter features taken together are about $400 \times 300\ m^2$ in extent. They may indicate two subsidence craters or a single crater of irregular form. Their location coincides with one of four possible test sites identified in 1996 by Gupta and Pabian [9] in their analysis of historical commercial satellite imagery. Also shown in the figure are details from a Russian KVR-1000 satellite image acquired on Feb. 2, 1998 and from a French SPOT panchromatic image acquired on May 13, 1998. The irregular "hammer-like" feature which gave rise to the third strong change signal is evident in the SPOT image. It is approximately 900 m long in its north-south extent and about 400 m wide. A very likely interpretation for this change is that a brush fire, spreading from north to south, was partially stopped by a road running north-west to south-east, but then continued in its central part beyond the obstruction before burning out, see Fig. 7. This feature is also quite weak in the second LANDSAT image. The strength of the corresponding change signal in the difference component illustrates the high sensitivity of the change detection technique.

Figure 7: Cutout from the SPOT panchromatic image acquired on May 13, 1998 with change detection.

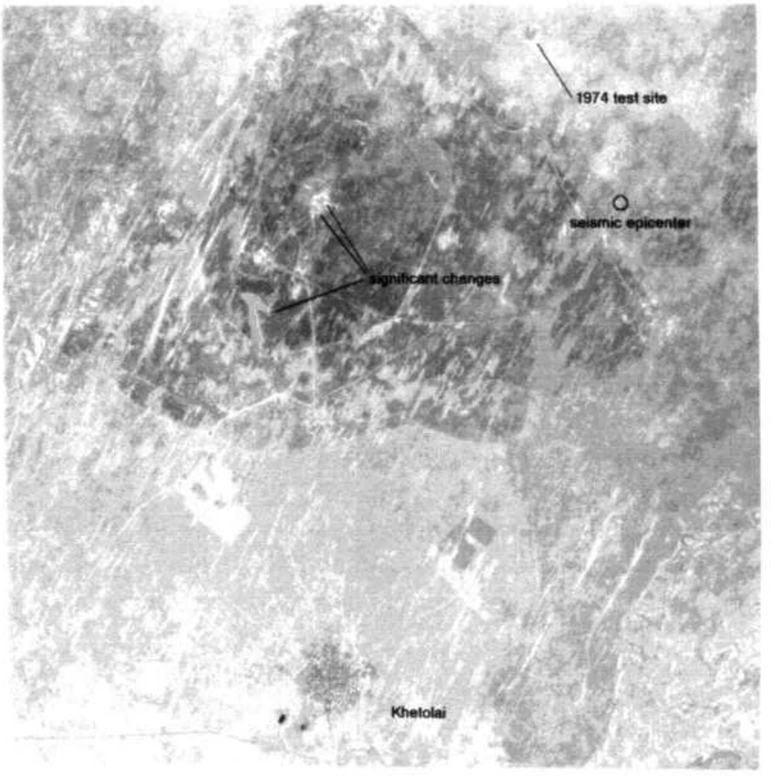

Figure 8: Overview of the Pokaran test area (SPOT panchromatic image from May 13, 1998) showing the significant changes as well as the seismic determination of the epicenter of the May 11, 1998 event and site of the May 18, 1974 underground nuclear test.

Fig. 8 shows an overview of the Pokaran area, indicating the three significant changes that were found as well as the site of the crater from the Indian underground nuclear explosion of 1974, as identified by Gupta and Pabian [9]. Using their published coordinates of the 1974 test site as a fixpoint, together with the georeferencing information supplied with the SPOT image, we place the center of the upper two change signals at 71.720E 27.079N. These coordinates are to be compared with the seismic determination of 71.761E 27.072N for the epicenter of the test (or tests) on May 11, also shown in the figure, as provided by the seismological monitoring stations of the prototype International Data Center (pIDC). Its separation from the detected test site is 4.1 km. The location of a nuclear test derived independently by change detection can be used as a seismic master event location for relative location of possible future explosions at the test site. In the present instance, the distance between the seismic and satellite location of 4.1 km points to a remarkably good localization capability for the IMS, considering the limited deployment of the network in 1998. It falls well within the quoted error ellipse with semi-major and semi-minor axes of 9.6 km and 8.4 km, respectively.

Recently the Federation of American Scientists have published on their website a qualitative analysis of panchromatic satellite imagery taken in June 1996 and February 2000 over the Pokaran area. They report that their findings are "not inconsistent" with an underground test at the position that we have identified in the present investigation. Ground truth photographs released by the Indian authorities after the tests, when compared with the KVR-1000 image (see Fig. 6), leave little doubt that this indeed was the site of the May 11 explosions.

3.1.2 Nevada

The Nevada nuclear test site is located some 100 km north-west of Las Vegas. The most recent tests were carried out at the Pahute Mesa, Rainer Mesa and Yucca Flats regions of the site. An underground test (code named *Contact*) was carried out at the Nevada site on 22.6.1989, and its coordinates were declared by the American authorities. The explosive was placed at a depth of 500 m, and the seismometer data suggested test was of a low yield weapon [8]. Two LANDSAT images were available, a LANDSAT 5 image from 21.6.1989 and a LANDSAT 4 image acquired only eight days later, on 29.6.1989. Change detection results are shown in Figures 9 and 10.

A strong signal (Fig. 9) is observed in the fourth MAD component, located about 2.5 km north of the declared test site. This is interpreted as a land slide caused by the nearby test (magnitude 5.3). Examination of the raw difference data in MAD component 1 (Fig 10) shows clear evidence of a change at the declared site as well. Here the magnitude of the changes is rather small, but the spatial coherence of the signals makes them quite apparent.

3.2 NPT verification

In May 1997, the Board of Governors of the International Atomic Energy Agency (IAEA), meeting in Vienna, passed a model protocol that was intended to improve and strengthen verification of the non-proliferation commitments of its member States. The key objective of the new measures agreed upon in the protocol is to enhance the IAEA's capability to detect possible

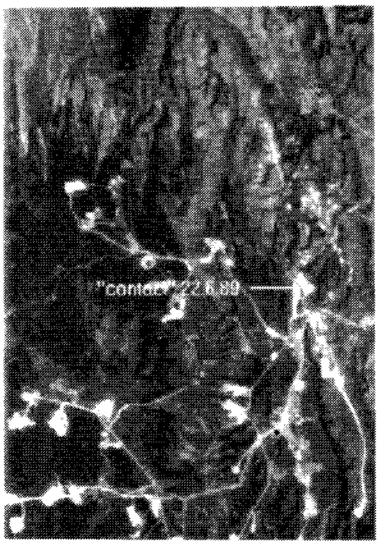

Figure 9: Change detection for Nevada test site for 21.6.1989 (LANDSAT 5) and 29.6.1989 (LANDSAT 4). The red pixels indicate the changes in MAD component 4 exceeding 3 standards deviations.

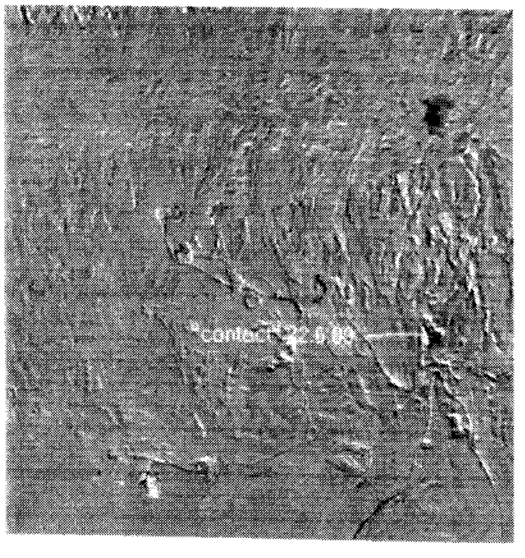

Figure 10: Change detection for Nevada test site for 21.6.1989 (LANDSAT 5) and 29.6.1989 (LANDSAT 4), MAD component 1. Pixel intensities differing from middle gray indicate degree of change

clandestine nuclear activities and thus to increase confidence that member States carry out their obligations. In addition to enhanced access for inspectors and extended routine declarations, these new measures will include the use of open-source information, collected with state-of-the-art technologies, to enable the IAEA to draw its conclusions more effectively and in a way that is transparent for the member States. One such open source of information is the vast amount of remote sensing data gathered by commercial satellites. The following two examples again illustrate some of the potential of change detection with commercial satellite imagery, this time for routine verification under the new protocol.

3.2.1 Bruce

Under a recent agreement with the Canadian Safeguards Support Program (CSSP) entitled "Collaboration between Germany and Canada on Detection of Changes using Thermal Infrared Imagery", the CSSP and its Canadian partner, the International Security Research and Outreach Program (ISROP) of the Department of Foreign Affairs and International Trade (DFAIT), have kindly provided us with a series of LANDSAT, IRS, IKONOS and RADARSAT images over the Bruce Nuclear Power Development (BNPD) facility on Lake Huron, Ontario. This facility is of course subject to routine safeguards measures under the Nuclear Non-Proliferation Treaty (NPT) and the available data provide a convenient basis for application of the change detection algorithm.[2]

The BNPD facility is situated on the eastern shore of Lake Huron between Port Elgin and Kincardine (see Fig, 11). It consists of nine reactor units, four (750MWe each) at Bruce A, four (840MWe each) at Bruce B and a prototype reactor (200MWe) at Douglas Point. Only the four units at the Bruce B site are operating at present. The shut down dates for the Bruce A units were: Unit 1 on 16.8.1997, Unit 2 on 8.8.1995, Unit 3 on 9.4.1998 and Unit 4 on 16.5.1998. The Douglas Point reactor has been de-commissioned. All reactors use natural uranium and heavy water, the latter being produced in a heavy water production plant situated in the same site.

A false color composite of the BNPD site is shown in Fig. 12. This LANDSAT 7 image was taken on 26.8.1999 and the cutout includes a good deal of

[2]Technical support and advice received from Bob Truong, CSSP, J.P. Paquette of Im-Strat Corporation, R. Keeffe, Head of the CSSP, J. Brauneisen, John Van Berlo of the Atomic Energy Control Board, and P. Baines of the DFAIT, are very much appreciated.

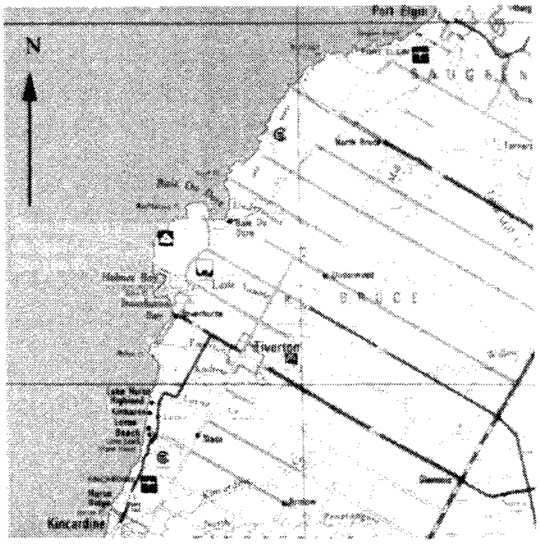

Figure 11: Map showing the Bruce Nuclear Power Development site on Lake Huron.

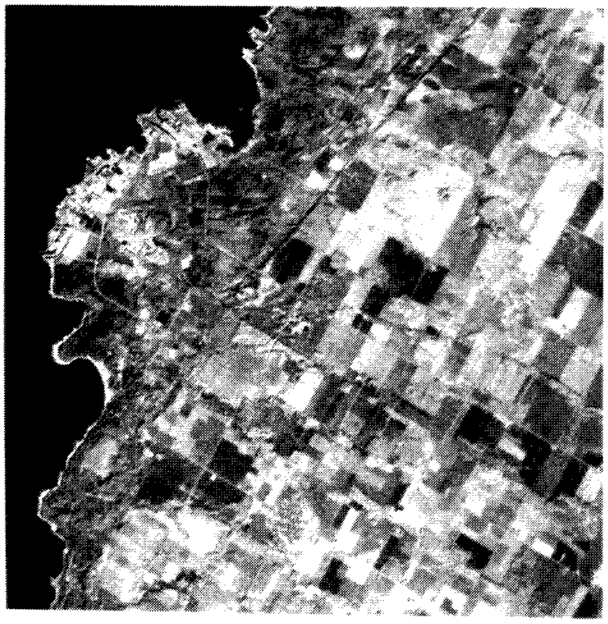

Figure 12: False color composite of the Bruce site and surroundings using the first, second and third principal components and the panchromatic channel of the LANDSAT 7 image from 26.9.1999.

surrounding countryside as well as lake water. The image is a combination of the first three principal components (in red, green and blue), which account for more than 99% of the spectral variance in the original 6 optical/infrared components, fused via the intensity-hue-saturation (IHS) transformation to the panchromatic channel, which has 15m ground resolution. Fig. 13 shows a section of a false color composite of an IKONOS-2 multispectral image from 11.11.1999, showing the area of Douglas Point reactor.

Figure 13: Pan-sharpened false color composite of the Bruce site using the first, second and third principal components in red, green and blue, respectively, of the IKONOS-2 image from 11.11.1999.

Four bitemporal/multispectral scenes (BMS) were produced from the available data:

- BMS1: August 1988 – August 1996, wide area
- BMS2: August 1988 – August 1996, BPND site only
- BMS3: August 1996 – May 1997
- BMS4 August 1996 – September 1999

Since only a single IKONOS image was available at the time of writing, all of the above involve LANDSAT images. Each BMS therefore consists of twelve spectral components, six for each time point. They were created by image-to-image registration with a second order polynomial mapping and nearest-neighbor resampling. The RMS registration error was approximately ±0.5 pixel.

In BMS1 and BMS2, due to the eight-year time difference, significant changes are to be expected at the site itself, whereas in BMS3 relatively large seasonal vegetation differences (late summer vs. spring) are likely to dominate. In 1999 the level of Lake Huron was considerably lower than previous years. This should lead to a clear change signal along the shoreline.

Fig. 14 shows two thresholded MAD components for BMS1 indicating the most significant changes. Note the separation of correlated changes into different colors. The changes indicated in green appear to be primarily associated with differences in water levels (shoreline of the lake or creation/drainage of ponds), those in red mainly with alterations in man-made structures and with land clearing or excavation. A number of significant changes are evident, both within and without the BNPD site. The removal of four of the six original heavy water production towers is clearly indicated, and some major changes have also taken place at the Bruce A and Douglas Point reactor. It was possible to interpret these from historical records for the site complex (see below). What appears to be a false signal is generated by the Douglas Point reactor itself and by two large oil storage tanks nearby. These three objects are extremely bright in both LANDSAT images and the false alarms may originate from saturation of the sensors in some, but not all, of the spectral channels. (The MAD procedure is a linear transformation, and non-linearities such as saturation will affect it adversely).

Fig. 15 shows a similar result for BMS2, fused to an IRS-1C panchromatic image from Sept. 1997. It should be emphasized that the MAD transfor-

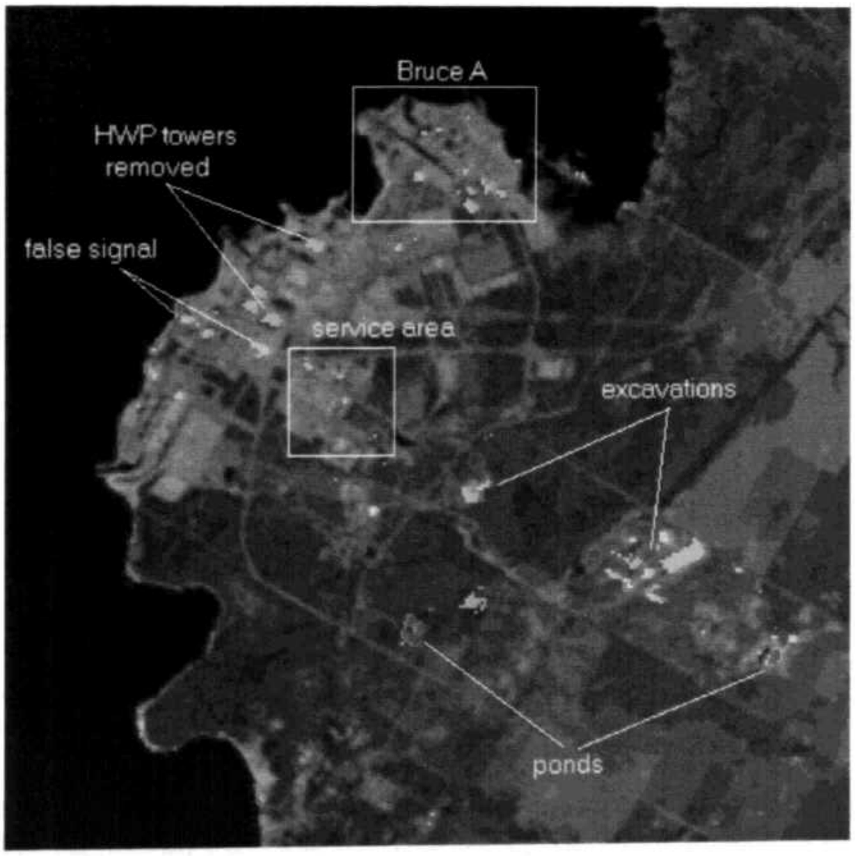

Figure 14: MAD change detection for BMS1 (August 1988 – August 1996). The first two MAD components exceeding approximately 2.5 standard deviations are in red and green. They are fused via the RGB–IHS transformation to channel 5 of the August 1988 image.

mation was recalculated using only the statistics of the image cutout shown here. Therefore some differences are to be expected relative to the wide area image of Fig. 14. The results for the two images are nevertheless quite similar. In addition to the removal of four heavy water production towers, changes are apparent in the Bruce A and Douglas Point reactor areas. These are due for instance to the construction of a parking lot and removal of a steam plant that was feeding the heavy water plants. The construction of a sewage treatment plant outside the facility proper, consisting of a pump house and four settling ponds, is seen clearly in the lower right hand corner.

In both Fig. 14 and Fig. 15, significant change detection thresholds were set automatically by the software.

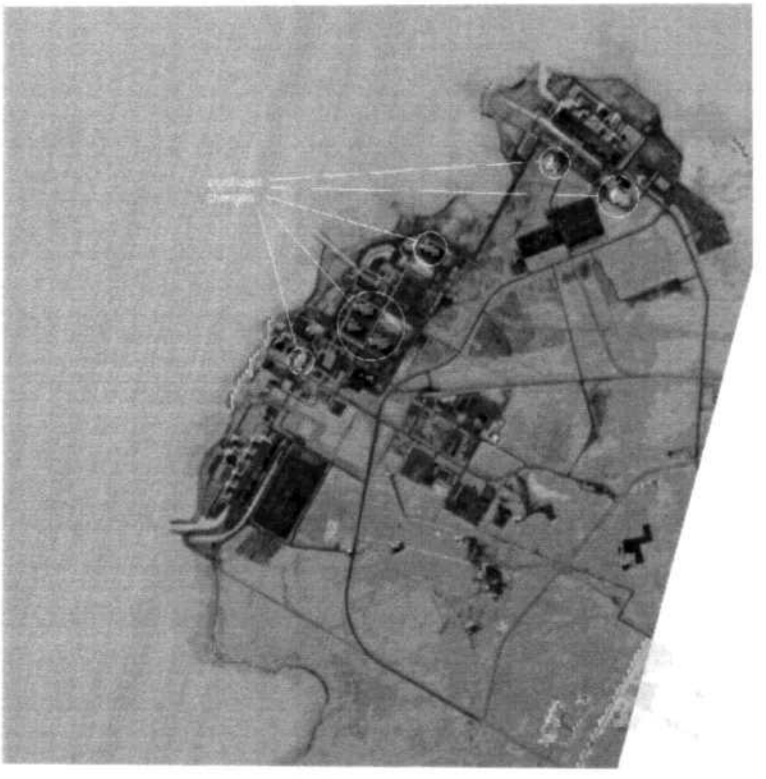

Figure 15: MAD change detection for BMS2 (August 1988 – August 1996) fused to the negative of an IRS-1C panchromatic image taken on 8.9.1997. The first two MAD components exceeding approximately 2.0 standard deviations are in red and green.

The change detection result for BMS3 is shown in Fig. 16. As expected, apart from the same false signals discussed above, no significant changes are apparent at the BPND site. The figure indicates a number of changes outside the site which are associated with differences in water levels or wetland.

Fig. 17 illustrates those large-scale changes associated with agricultural land use in BMS1. These are the kind of changes that the MAD procedure was originally designed for, and it shows them very well. In this case all six MAD components have been further processed by another orthogonalization based on the autocovariance of the multispectral image (the so-called maximum autocorrelation factor (MAF) analysis [1].) This transformation has the effect of improving the spatial coherence of the change detection signals and allows most of the information to be combined into a singe false color composite image, as was done here. Finally, the drop in the level of the lake expected

Figure 16: MAD change detection for BMS2 (August 1996 - May 1997). The first two MAD components exceeding approximately 2.2 standard deviations are in red and green. They are fused via the IHS (intensity-hue-saturation) transformation to channel 5 of the May 1997 image for better reference.

in BMS4 is clearly signaled in Fig. 18.

3.2.2 Wismut

As an example for verification of uranium mining, as declared under the new Protocol, the change detection methods were applied to the open pit mine Lichtenberg near Ronneburg/Gera, in eastern Germany, in an area currently being reclaimed by the Federal Government.

After German re-unification in 1990, Germany and the then Soviet Union agreed to the shutdown of uranium mining operations in eastern Germany. Since then, the public corporation Wismut GmbH has been concerned exclusively with reclamation and re-cultivation of the various mining areas in-

Figure 17: MAD/MAF analysis for BMS1 showing the first three MAF components in red, green and blue, fused to channel 5 of the 1988 image. The significance thresholds are set at one standard deviation. The MAF orthogonalization enhances the spatial coherence of the MAD result.

volved. In this example a bi-temporal change detection analysis was done on the basis of two Landsat TM scenes acquired on the 3.8.1990 and 11.6.1997. We fused a high-resolution KVR-1000 image[3] to the MAD components. Ground control was derived from airborne images taken by the Wismut GmbH at the same period.

Fig. 19 shows a result for the open pit mine Lichtenberg with automatic thresholds for MAD 1 and MAD 2. The interpretation of the changes are listed in figure caption. All of the indicated changes were assigned to the Wismut properties/area. Because of the lack of background information it was not possible to associate the changes (D) to (H) accurately, but the changes in the area of uranium mill could definitely be identified.

[3] Taken from a CD-Rom which is commercially available in Germany (D-Sat2).

Figure 18: MAD change detection for BMS4 (August 1996 – September 1999). The first component exceeding 1.5 standard deviations is shown green. It is fused via the IHS (intensity-hue-saturation) transformation to the 15m resolution panchromatic channel of the 1999 image.

In order to extract change information which was not identified in the first image, we set the threshold to one standard deviation. Thus, the false positive probability increased considerably and, also, more changes were recognizable which were not of interest. However some very interesting ones appeared, see Fig. 20.

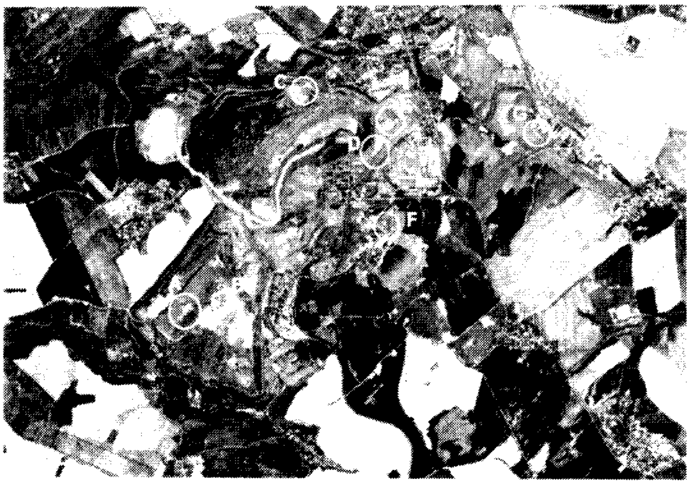

Figure 19: The open pit mine Lichtenberg, showing MAD components 1 and 2 from LANDSAT scenes taken on 3.8.1990 and 11.6.1997 with thresholds set automatically (approximately 2.5 standard deviations). By correlation with ground truth data, the following changes could be interpreted: A: zone where material from waste rock piles was removed, B: dried up pond, C: clay was piled up for the reclamation in the early 90s, D–H: reclamation of the uranium mill tailing.

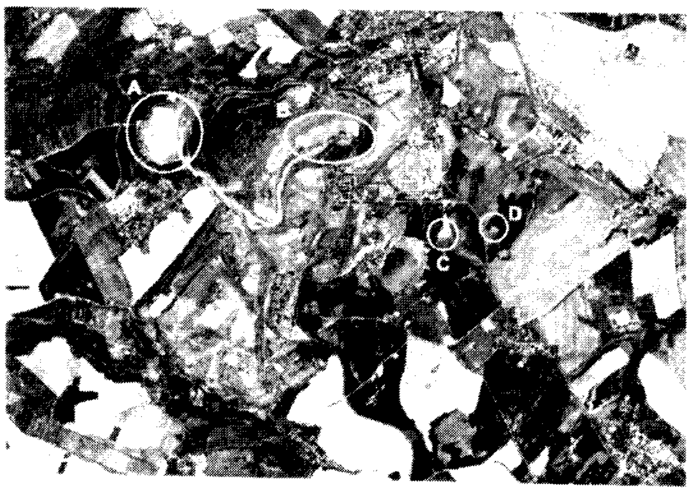

Figure 20: As Fig. 19, but with significance thresholds set at one standard deviation. Additional changes identified from ground truth were: A: movement of "Gassenhalde" to the Lichtenberg pit, B: waste rock piles dumped into the open pit, C: tearing down of a tax mixing facility, D: removal of "shaft 380".

3.3 FMCT verification

The next important international effort to control the production of fissile material is likely to be a Fissile Material Cutoff Treaty (FMCT). After it enters into force, many weapons production facilities will declared and then shut down, so that the primary aim of verification is likely to be the confirmation of the status of such facilities. Moreover, according to a recent assessment by Zhang [10]:

> ... an FMCT also needs to develop techniques to detect undeclared nuclear facilities. To reduce concerns about potential loss of sensitive information at defense-related nuclear processing sites, it is desirable to apply less intrusive verification measures – satellite imagery.

The following investigations involve both a declared and an undeclared weapons facility. They were carried out in close collaboration with Bhupendra Jasani, Dept. of War Studies, King's College London. Images of the plutonium production site at Hanford were kindly made available by the American IAEA Support Program.

3.3.1 Hanford

The Hanford complex was established as part of the Manhattan Project. It is situated in the state of Washington, between the Columbia River and the Yakima and Snake Rivers, occupying an area of about 1500 km^2. All plutonium production reactors are located along the Columbia River. Between 1943 and 1945, three reactors based on the Oak Ridge pilot reactor and three reprocessing plants for plutonium separation were constructed. Five more reactors, two replacement reprocessing facilities and 81 underground waste storage tanks (in addition to an original 64) were also constructed between 1947 and 1955.

Three satellite images are analyzed here: two LANDSAT 5 images from 12.8.1983 and 28.6.1987 for change detection, and one IRS-1C panchromatic image from 7.7.1997. Identification of individual reactors was not possible in the LANDSAT images because of the poor resolution. Also, the thermal band of the LANDSAT images indicated no discharge of warm water into the river, suggesting that the reactors were not in operation at the time of data acquisition.

Figure 21: False color composite of the LANDSAT image of the Hanford site from 28.6.1987, bands 3 (blue), 4 (green) and 5 (red).

Figure 22: MAD change detection for LANDSAT images of Hanford from 12.8.1983 and 28.6.1987. Components 1 and 2 are shown in red and green, respectively. The thresholds are set at approximately 2 standard deviations. The background image is band 5 of the 1987 scene.

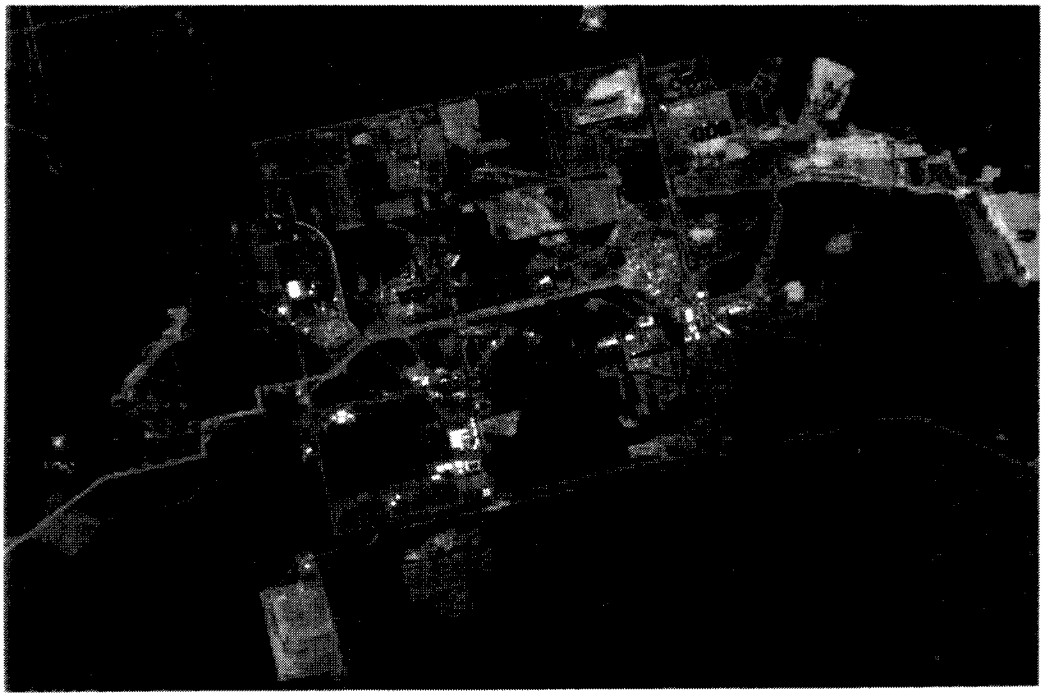

Figure 23: Close up of a service area at Hanford. MAD components as in Fig. 15, registered and fused to the IRS-1C panchromatic image from 7.7.1987 having a spatial resolution of 5m.

Fig. 21 shows an overview of the entire site in the form of a false color composite of the 1987 LANDSAT image. Change detection results are shown in Fig. 22 and Fig. 23. Again we observe a good discrimination of changes, many associated with natural phenomena (river levels, dried up lakes, etc.)

Since this is a military establishment, accurate ground truth information is not readily available. However most of the human activity, apart from the possible construction of a small air strip at one of the reactors and agricultural changes outside the site, appears to be associated with excavations and drillings for waste disposal sites.

3.3.2 Kushab

Pakistan, which is not a member of the NPT, has unsafeguarded facilities throughout its nuclear fuel cycle capable of feeding uranium enrichment plants and providing fuel for its nuclear reactors [11]. The site at Kushab, for example, located in the north-eastern part of the country, consists of a heavy water reactor and associated heavy water production plant. According to a recent analysis by the Federation of American Scientists (FAS) [12]:

> The heavy water research reactor at Khushab is a central element of Pakistan's program for production of plutonium and tritium for advanced compact warheads. The Khushab facility, like that at Kahuta, is not subject to IAEA inspections. Khushab, with a capacity variously reported at between 40 MWT to 50 MWT [and as high as 70 MWT], was "commissioned" in March 1996, and had been under construction with Chinese assistance since the mid-1980s.

In order to test the change detection algorithm at the relatively high spatial resolution of 4m, two IKONOS images of the site were purchased. The first, taken on 22.2.2000, was the archived image used by the FAS in its analysis. It consisted of both 4 multispectral bands (visible blue, green red and near infrared) with 4m spatial resolution and the corresponding panchromatic image with 1m spatial resolution. The following is an excerpt from the provider's data:

```
Scan Direction:  0 degrees
Nominal Collection Azimuth:  346.3675 degrees
Nominal Collection Elevation:  63.90105 degrees
Sun Angle Azimuth:  145.4341 degrees
Sun Angle Elevation:  41.03904 degrees
Acquisition Date/Time:  2000-02-22 05:41
```

The second image was acquired on 25.5.2000 and consisted of the 4 multispectral bands only:

```
Scan Direction:  0 degrees
Nominal Collection Azimuth:  78.5415 degrees
Nominal Collection Elevation:  74.62959 degrees
Sun Angle Azimuth:  111.6230 degrees
Sun Angle Elevation:  66.40987 degrees
Acquisition Date/Time:  2000-05-25 05:34
```

The total area covered was approximately 160 km^2. Although the acquisition times were very similar, the first image was considerably off nadir and, due to the lower (winter) sun angles, exhibited considerably longer shadows than the second image. The data were supplied in 11 bit resolution. They were reduced to 8 bit resolution after contrast enhancement for further analysis. Fig. 24 shows a false color composite overview of the site at 4m resolution, with the research reactor at the top and the heavy water production plant complex near the bottom.

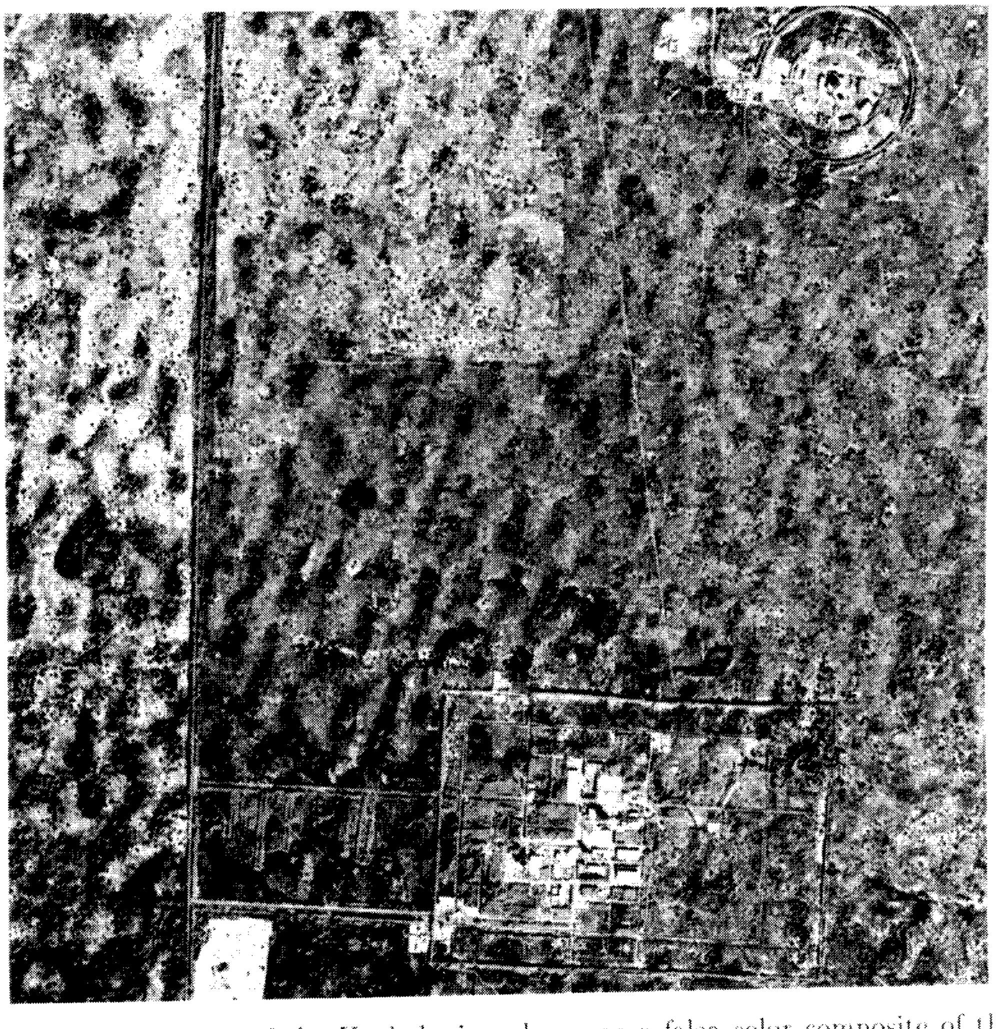

Figure 24: Portion of the Kushab site, shown as a false color composite of the multispectral IKONOS image from 22.2.2000, band 1 (blue) band 2 (green) band 4 (red). The spatial resolution is 4m.

Fig. 25 shows the result of change detection applied to part of the heavy water plant, fused to the panchromatic image for better interpretation. No anthropomorphic changes can be identified. (This was the case for all other parts of the site, as well). The MAD components discriminate differences due to shadows and changes in vegetation quite well.

Figure 25: MAD change detection for the IKONOS images from 22.2.2000 and 25.5.2000 for part of the heavy water plant site. The first MAD component (blue) detects the changes in building shadows, the second MAD component (red) is mainly associated with changes in green vegetation. The difference images have been fused to the panchromatic image from 22.2.2000 with a spatial resolution of 1m.

Fig. 26 shows the simulation of a man-made change. One of the service buildings was copied to an area slightly to the east. Not surprisingly, this creates a very strong change signal, in this case in the fourth MAD component (green).

Figure 26: As Fig. 25, with simulated construction of a service building (green, MAD component 4).

4 Conclusions

The CTBT case studies have demonstrated the usefulness of combined seismic and satellite image analysis for CTBT verification. The LANDSAT imagery, when used in change detection mode, is ideally suited to locate signals of the typical dimensions of a spall zone in very large scenes. Higher resolution data, if available, can then be consulted to aid in the interpretation of the change signal. The observation of a possibly significant change in satellite imagery, in conjunction with a seismic signal, could be used to trigger and to guide on site inspections by the CTBT control authority.

With regard to routine verification of the NPT, multi-spectral change detection is a potentially useful tool to focus attention on facility design changes that may be safeguards relevant. The time resolution in the satellite imagery used in the investigations described here was inadequate to make definitive statements. Most of the interesting changes at the Bruce site, for instance, occurred in the 8-year interval spanned by the 1988 and 1996 LANDSAT images. Moreover at a spatial resolution of 30m, many relevant changes may go undetected. Change signals of the order of one or two pixels in extent are suspect as well, as they may be artifacts of the image-to-image registration. It is therefore intended to apply the algorithm to high resolution multi-spectral images (such as shown in Fig. 8) as soon as bitemporal data become available.

The applicability of high resolution imagery for the observation of unsafeguarded or undeclared nuclear facilities in connection with an FMCT is obvious. Whether or not change detection is useful at $\leq$ 4m resolution remains to be seen. The Kushab images demonstrate the disturbing effects of shadows from trees and buildings, which can complicate interpretation of change signals at such resolutions. The capability of the MAD method to separate shadow formation from other changes might be of considerable advantage in this regard. The use of object-oriented, hierarchical segmentation of the differenced imagery offers a promising method of masking shadow effects. The classification system *eCognition* of Definiens AG Munich is currently under investigation in this connection.

The MAD algorithm takes advantage of the spectral discrimination in the 4m multispectral bands of Ikonos imagery. The 1m panchromatic information is not used. The ARSIS concept [13] for resolution enhacement using wavelet fusion techniques allows inclusion of the high resolution information into the multivariate change detection calculation. It is being integrated into the CDSat software.

The Hanford images, on the other hand, illustrate in particular the advantage of performing change detection for very large sites using relatively poor spatial resolution LANDSAT data. One obtains very quickly a compact overview of the entire area and can pinpoint possible change signals of relevance to nuclear verification. Of course, their further interpretation requires access to higher resolution imagery (as in Fig. 23) or to collateral information.

A Software implementation

CDSat (Change Detection with Satellite imagery) is a graphical environment for examining changes in multispectral satellite images. It implements the *multivariate alteration detection* (MAD) method proposed by Alan Nielsen and co-workers in 1998 [1] and described in detail in this report. In addition it implements automatic significance threshold determination, contour and corner matching algorithms for the determination of ground control points for fast image-to-image registration as well as the ARSIS wavelet fusion model for resolution enhancement of multispectral channels [13]. It adheres to the PCIDSK image file format used by PCI/Geomatics Inc. and therefore can run as an extension module for their EASI/PACE(c) image processing software.

CDSat is written in Object Pascal with the rapid application development environment DELPHI(c) of Borland/Inprise Corp. Currently it is available on CD-ROM for the Windows 95/98/NT/2000 operating systems (for more information, contact the author: `m.canty@fz-juelich.de`).

B Publications

M. J. Canty and J. Schlittenhardt, Locating the 1998 Indian nuclear tests, *Eos* 82(3), 2001, pp. 25–29.

M. J. Canty, B. Jasani and Q. S. B. Truong, Satellite imagery for nuclear safeguards: the Bruce Nuclear Power Development Site, *Proceedings of the 22nd Annual ESARDA Meeting*, Dresden, May 8-12, 2000.

S. Kreft, M. Canty, G. Menz, Change detection: Using Landsat images to observe a uranium mine, *Proceedings of the 4th Annual FLINS Conference*, World Scientific, 2000, pp. 263–268.

References

[1] Nielsen, A. A., Conradsen, K. and Simpson, J. J., Multivariate alteration detection (MAD) and MAF processing in multispectral, bitemporal image data: New approaches to change detection studies, *Remote Sens. Environ.* 64(1), 1998, pp. 1–19.

[2] Wiemker, R., An iterative spectral-spatial bayesian labelling approach for unsupervised robust change detection on remotely sensed multispectral imagery, in G. Sommer, K. Daniilidis and J. Pauli (eds.) *Proceedings of the 7th International Conference on Computer Analysis of Images and Patterns*, Springer LNCS Vol 1296, pp. 263-270, Heidelberg, 1997.

[3] Bruzzone, L., Prieto, D. F., A Bayesian Approach to Automatic Change Detection, *Proc. of the IEEE 1999 Int. Geoscience and Remote Sensing Symposium (IGARSS99)*, Hamburg, Germany, 28 June-2 July, 1999, Vol. III, pp. 1816–1818.

[4] Bishop, C. M., *Neural Networks for Pattern Recognition*, Oxford University Press, 1995.

[5] Li, H., Manjunath, B. S., Mitra, S. K., A contour-based approach to multisensor image registration, *IEEE Transactions on Image Processing* 4(3), 1995, pp. 320–334.

[6] Zitova, B., Kautsky, J., Peters, G., Flusse, J., Robust detection of significant points in multiframe images, *Pattern Recognition Letters* 20, 1999, pp. 199–206.

[7] Richards, J. A., *Remote Sensing Digital Analysis*, Springer, 1993.

[8] Jasani, B., Verification of a comprehensive test ban treaty from sapce: A prliminary study, Research Paper No. 32, UNIDIR/94/46, United Nations, New York, 1994.

[9] Gupta, V., Pabian, F., Investigating allegations of Indian nuclear test preparations in the Rajasthan Desert, http://www.ca.sandia.gov/casite/gupta/index.html.

[10] Zhang, H., Potential applications of commercial observation satellite imagery for the verification of declared and undeclared nuclear production facilities, INMM Meeting, New Orleans, 2000.

[11] Koch, A., Topping, J., Pakistan's nuclear weapons program: A status report, *The Nonproliferation Review*, Vol. 4, No. 3, 1997.

[12] Federation of American Scientists Website, `www.fas.org/nuke/guide/pakistan`

[13] Ranchin, T., Wald, L., Fusion of high spatial and spectral resolution images: the ARSIS concept and its implementation, *Photogrammetric Enginerring and Remote Sensing* 66(1), 2000, pp. 49–61.

Forschungszentrum Jülich

Jül-3842
January 2001
ISSN 0944-2952